Biogeosciences Discuss., 9, 12505–12542, 2012
www.biogeosciences-discuss.net/9/12505/2012/
doi:10.5194/bgd-9-12505-2012

Biogeosciences Discussions

Inferring past land-use induced changes in surface albedo from satellite observations: a useful tool to evaluate model simulations

J. P. Boisier, N. de Noblet-Ducoudré, and P. Ciais

Institut Pierre Simon Laplace, CNRS/INSU – Laboratoire des Sciences du Climat et de l'Environnement, UMR8212, Gif-sur-Yvette, France

Received: 30 July 2012 – Accepted: 20 August 2012 – Published: 14 September 2012

Correspondence to: J. P. Boisier (juan-pablo.boisier@lsce.ipsl.fr)

Published by Copernicus Publications on behalf of the European Geosciences Union.

Abstract

Cooling resulting from increases in surface albedo has been identified in several studies as the main biogeophysical effect of past land-use induced land cover changes (LCC) on climate. However, the amplitude of this effect remains quite uncertain due to, among other factors, (a) uncertainties in the magnitude of historical LCC and, (b) differences in the way various models simulate surface albedo and more specifically its dependency on vegetation type and snow cover. We have derived monthly albedo climatologies for croplands and four other land-cover types from MODIS satellite observations. We have then estimated the changes in surface albedo since preindustrial times by combining these climatologies with the land-cover maps of 1870 and 1992 used by modelers in the context of the LUCID intercomparison project. These reconstructions show surface albedo increases larger than 10 % (absolute) in winter and 2 % in summer between 1870 and 1992 over areas that have experienced intense deforestation in the northern temperate regions. The MODIS-based reconstructions of historical changes in surface albedo were then compared to those simulated by the various models participating to LUCID. The inter-model mean albedo response to LCC shows a similar spatial and seasonal pattern to the one resulting from the reconstructions, that is larger increases in winter than in summer driven by the presence of snow. However, individual models show significant differences with the satellite-based reconstructions, despite the fact that land-cover change maps are the same. Our analyses suggest that the primary reason for those discrepancies is how land-surface models parameterize albedo. Another reason, of secondary importance, results from differences in the simulated snowpack. Our methodology is a useful tool not only to infer observations-based historical changes in land surface variables impacted by LCC, but also to point to major deficiencies within the models; we therefore suggest that it could be more widely developed and used in conjunction with other tools in order to evaluate global land-surface models.

BGD
9, 12505–12542, 2012

1 Introduction

Human-induced land-cover change (LCC) has modified large portions of the natural landscape since pre-agricultural times, and deforestation has been particularly extensive in the Northern Hemisphere temperate regions (Hurtt et al., 2006). Surface albedo is a key element in LCC-related climate change studies as it controls the magnitude of energy absorbed by land-surfaces, which heats the land and drives turbulent fluxes. In temperate latitudes, non-forested lands reflect about 5 % (absolute) and 30 % more solar radiation than forests in respectively snow-free and snow-covered conditions (Jin et al., 2002; Gao et al., 2005).

As spatially coherent global observations of land-surface properties only exist for the satellite period, impacts of large-scale historical LCC have been principally assessed using global climate models (GCMs) instead of observations. Most of these numerical results show that past LCC has principally led to cooling in the northern extratropics through the increase in surface albedo. This albedo-induced cooling opposes the warming induced by non-radiatively processes that in contrast tend to predominate at lower latitudes (e.g. Gowindassamy et al., 2001; Bounoua et al., 2002; Feddema et al., 2005; Betts et al., 2007; Kvalevag et al., 2010; Davin and de Noblet-Ducoudré, 2010). Changes in surface albedo have usually been characterized and quantified by means of the radiative forcing concept, in order to compare LCC to other climate forcings (Hansen et al., 1998; Betts, 2001; Matthews et al., 2003; Myhre and Myhre, 2003; Betts et al., 2007; Davin et al., 2007; Forster et al., 2007).

Myhre et al. (2005) estimated the LCC-induced changes in surface albedo and the resulting radiative forcing based on present-day observations of albedo using the Moderate Resolution Imaging Spectroradiometer (MODIS) data. Their results show weaker albedo changes than other published numerical studies, in part because of the lower MODIS-derived crops albedo values.

In the context of the "Land-Use and Climate: Identification of robust Impacts" (LUCID) project (Pitman et al., 2009), a coordinated set of simulations was realized using seven

BGD
9, 12505–12542, 2012

GCMs to evaluate the robust biogeophysical impacts of LCC since the preindustrial period. All simulations were forced with observed sea-surface temperatures and sea-ice, CO_2 concentrations, and two land cover distributions: one for preindustrial times (year 1870) and one for present-day (year 1992). One robust result is that LUCID models systematically simulate increases in surface albedo in response to LCC changes between preindustrial and present-day. Although in most models the near surface cools down throughout the year, some simulate seasonal warming due to a dominant impact of the non-radiative effects (de Noblet-Ducoudré et al., 2012). Although the simulated change in surface albedo shows a common direction, its magnitude varies significantly from one model to the other. Such variability has two main causes, as discussed in Boisier et al. (2012): differences in land-surface model (LSM) albedo sensitivities to LCC and differences in land-cover maps prescribed in each LSM. Although all models used the same crop and pasture extents for both years 1870 and 1992, modelers have implemented them using different procedures into their own standard vegetation maps. This has induced significant differences in the deforestation rates that each model deduced between the preindustrial times and present-day (ranging from ~ 4 to 10 million km^2) and, therefore, in the simulated responses to LCC in e.g. surface albedo.

It is rather difficult to disclose one of the LUCID vegetation' reconstructions as there are many uncertainties in identifying what has been the "real" anthropogenic LCC. One results from the reconstruction of the historical record of cropland and pastureland, while another may come from current land cover characterization as discussed in Feddema et al. (2005) and de Noblet-Ducoudré et al. (2012). Moreover, we often know little about the specificities of land conversion to croplands (i.e. deforestation or conversion from previously grass-covered area) although some initiatives have started to address this issue (e.g. Hurtt el al., 2006). With respect to the surface albedo's sensitivity to LCC, variations between models result from the snow cover simulated and different land-surface parameterizations, notably, the one used for cropland albedo (Matthews et al., 2003; Myhre and Myhre, 2003). The realism of this sensitivity should be assessed using datasets. This is what we are trying to do in this paper.

BGD
9, 12505–12542, 2012

In this study we develop a new tool (Sect. 2) to reconstruct changes in surface albedo since the preindustrial period using satellite data, and following a methodology somewhat close to that of Myhre et al. (2005). The MODIS global albedo dataset is used to assign seasonally and spatially varying albedo values to different land cover types under snow-covered and snow-free conditions. This information is then combined with land cover and snow cover maps to reconstruct albedo climatologies. After an evaluation of the methodology adopted (Sect. 3.1), we estimate the albedo response to the different scenarios of land conversion used within the LUCID project (Sect. 3.2). We then evaluate the LUCID model's albedo sensitivity to changes in vegetation in relation to their simulated snow cover (Sect. 3.3). We finally evaluate the impacts of LCC in the net solar radiation at the surface based on the simulated and reconstructed albedo changes (Sect. 3.4). Discussion and conclusion are presented in Sect. 4.

2 Material and methods

The datasets used in this study gather a number of satellite-based data and global simulations from the LUCID model intercomparison project (Table 1). The shortwave broadband directional hemispherical reflectance (black-sky albedo)/snow cover (MCD43C3; Schaaf et al., 2002) and land cover (MCD12C1) products from MODIS were used to derive snow-free and snow-covered albedos of different land cover types. The National Snow and Ice Data Center (NSIDC) snow cover data (Armstrong et al., 2007) was used, in combination with present-day and pre-industrial LUCID vegetation maps, to reconstruct the surface albedo climatology of both time periods.

The set of LUCID simulations assessed here are 30-yr runs carried out in ensemble mode (5 members) by seven global climate models (GCMs), forced with monthly varying sea-surface temperature and sea ice concentration (from 1970 to 1999) and atmospheric CO_2 concentration (set to 375 ppm). Two types of simulations were computed to assess the impacts of LCC from the preindustrial (PI) period to present-day (PD), which only differ by the land cover maps prescribed in each model, representing

BGD
9, 12505–12542, 2012

the vegetation of 1870 in one case and that of 1992 in the other. For more details on the modeling experiment carried out within LUCID see de Noblet-Ducoudré et al. (2012). The list of GCMs, the associated land surface models (LSMs; hereafter GCM/LSMs) and their references are provided in Table 1.

Figure 1 summarizes our methodology for constructing the albedo climatologies. To start with, the black-sky albedo, snow cover and land cover data from MODIS were used to assign albedo values to four groups of vegetation (crops, grasses, evergreen trees and deciduous trees), in addition to bare soil. These five land cover groups (LCGs) were defined in order to have a comparable land cover partitioning between the MODIS data and the vegetation maps of the various LSMs assessed here. As the definition of vegetation varies from one model to another, this grouping ensures consistency when comparing the various reconstructions.

From the 5.6-km resolution MODIS dataset (0.05-degree latitude-longitude grid), climatological (2000–2011) monthly snow-covered and snow-free albedo maps for each of the five LCGs were derived by the means of global interpolation of grid-cells values showing a dominant fractional area of the selected LCG. Those grid-cells were defined as the ones showing LCG's fractions of 95 % or larger in MODIS land cover. Croplands dominate over large regions in North America, Eurasia and India (Fig. 2a). Grasses also dominate over extensive areas such in the North American Great Plains, in central Eurasia or in the Sahelian band. Evergreen trees are the major LCG in tropical rainforest and in some areas of boreal forest. Deciduous trees dominate in some areas such as in northeastern Eurasia, in eastern North America or in central South America. Besides desert regions, grid-cells with a dominant fraction of barren soil are sparsely found in other regions of the globe.

The albedo values of the dominant LCG's grid-cells were globally mapped by simple interpolation, using the spatially nearest value method. The resulting monthly mean albedo maps were then degraded from the 0.05-degree grid to a 2.0-degree grid, the standard one used to combine and compare the ensemble LUCID simulations with satellite data. This method allows capturing the spatial and seasonal albedo variability

BGD
9, 12505–12542, 2012

of each LCG resulting, among other causes, from the plant life-form heterogeneity (e.g. broad-leaved vs. needle-leaved plants) or from the leaf area index (LAI) distribution within the concerned LCG.

In a second step, global maps of "data-driven" albedo were reconstructed combining (a) each LUCID GCM/LSM specific land cover map of 1870 and 1992, (b) the LCGs' albedo data derived from MODIS observations and (c) the monthly NISDC snow cover from 1979 to 2006. We used the NISDC snow cover data instead of the MODIS ones because of its larger period availability (large enough for a robust climatology), and time coherency with LUCID simulations that cover the 1970–1999 period (see Table 1). The net albedo of a grid-cell (at 2.0-degree resolution) is calculated as follows:

$$\alpha = \sum_{v} F_v[(1-f)\,\alpha_v^{\mathrm{sf}} + f\,\alpha_v^{\mathrm{s}}], \quad (1)$$

where α_v^{sf} and α_v^{s} are respectively the MODIS-derived snow-free and snow covered albedos of the LCG v. F_v is the grid area fraction of LCG v, and f is the snow cover fraction of the corresponding grid-cell, assumed to be independent of LCG.

Figure 2b illustrates the forest fraction difference between 1870 and 1992 imposed in the various LUCID GCM/LSMs (model mean). Deforestation dominates the historical LCC, notably in the northern temperate regions where the forest fraction decrease is larger than 30 % (absolute) over extensive areas. Although the sign and the spatial pattern of the LCC agree within the various models, the strength of the resulting deforestation varies widely between them, because of the different strategies adopted by modelers to incorporate the prescribed historical crop and pasture data into the native land cover maps (de Noblet-Ducoudré et al., 2012).

In summary, 28-yr monthly albedo maps (period determined by the availability of the NSIDC snow cover data) were computed for the preindustrial (1870) and present-day (1992) land cover maps of each of the seven LUCID GCM/LSMs. Both time periods are assumed here to have experienced the same snow-cover distribution (the present-day one from NISDC), so that the resulting albedo difference between them only takes into

BGD
9, 12505–12542, 2012

account the direct LCC-induced change (i.e. in contrast to the indirect LCC impacts in albedo through changes in, e.g. snow cover). Differences between the reconstructed (data-driven) albedos and those simulated by each GCM/LSM are used in the following to assess the models' parameterizations and its resulting albedo sensitivity to LCC.

In order to evaluate the skill of the method used (Sect. 3.1), another reconstructed albedo dataset was established in the same way described above, but using consistently the 12-yr land cover and snow cover data from MODIS instead of the LUCID land cover maps and the NSIDC snow cover. Hence, since this reconstruction only uses information from MODIS, its difference with the MODIS albedo climatology measures the error of our methodology in scaling up the subset albedo data from grid-cells with dominant vegetation.

3 Results

3.1 Method evaluation: reconstruction of the present-day MODIS-based albedo

The northern winter (DJF) and summer (JJA) mean albedo of the northern temperate (30–60° N) subset of the grid-cells used to derive the LCG's albedo maps are summarized in Table 2. For DJF both the snow-free and the snow-covered mean albedos are given. The mean albedo values of the four vegetation classes defined by the LCGs generally agree with previous results derived from MODIS (Jin et al., 2002; Gao et al., 2005; Myhre et al., 2005; Cescatti et al., 2012). In summer, the snow-free albedo of crops and grasses are similar to each other (~ 0.15), and exceeds by near 0.06 and 0.03 those of evergreen and deciduous trees, respectively. As highlighted by Myhre et al. (2005), the mean snow-free albedo of croplands derived from MODIS (around 0.15 in this study) is lower than the standard values used in previous studies (e.g. Matthews et al., 2003). The recent MODIS albedo evaluation by Cescatti et al. (2012) have shown a good agreement between the satellite retrievals and in situ measurements, although a systematic underestimation in the MODIS-based albedo of herbaceous ecosystems

BGD
9, 12505–12542, 2012

with respect to the one observed in situ. They pointed out that these differences come from the landscape heterogeneity within these land-cover units (crops and grasses) and the resulting scale mismatch between the remote and in situ observations.

The snow masking effect exerted by forest compared to that of herbaceous plants is noteworthy (Table 2). In the case of evergreen trees, the snow-covered winter albedo averages 0.22, almost three times lower than that resulting for grasses and crops (~ 0.6).

In order to evaluate the skill of our global albedo reconstruction methodology, we have compared the reconstructed albedo fields based on the 2000–2011 MODIS land-cover and snow-cover data to the original MODIS albedo (Fig. 3). The global albedo patterns of January and July from MODIS (Fig. 3a and b) are generally well reproduced by the reconstructions (Fig. 3d and e). These patterns are characterized by relatively high albedo (larger than 0.3) over deserts and snow-covered areas, notably in the northern mid and high latitudes in January. By contrast, regions with closed forest show albedo values below 0.13, such as tropical rainforest or in boreal forest in July.

More specifically, the difference between the reconstructed and the observed mean albedo shows relatively small biases (< 0.01) in most land areas of the globe (Fig. 3c and f). Substantial differences are however observed in some regions such as in western and northern North America, in mid-Eurasia, in northern tropical Africa and in Australia. Most of these regions show rather large errors throughout the year (not shown) and correspond to areas for which, at the 5.6-km resolution MODIS land-cover data, very few grid-cells with more than 95 % of one specific LCG were found (Fig. 2a). Therefore, in these regions of heterogeneous biogeography, the albedo values of each LCG were interpolated from values over remote regions, with potentially different species and soil colors.

The observed MODIS albedo is particularly overestimated by the reconstruction in Eurasia in January (~ 15 %, relative), in central Africa in January (~ 30 %) and in Australia in both January and July (~ 25 %). The large positive bias of the reconstruction in Africa and Australia are particularly driven by their assigned barren soil albedos, which

BGD
9, 12505–12542, 2012

play a major role in these regions (i.e. they held open vegetation biomes), and were derived from extremely arid regions with high albedo located near them. These errors are important and could induce misleading estimates of LCC-induced albedo changes in regions where the latter are of the same order the corresponding bias. However, for the purpose of this study, the regions affected by the historical land use changes are principally located in the northern temperate regions, in areas with low bare soil fraction and small reconstruction errors (see solid contours in Fig. 3c denoting the regions in which the prescribed deforestation between 1870 and 1992 exceeds 10 % of land fraction).

Figure 4 shows the mean seasonal cycle of the MODIS observed and reconstructed albedo averaged over the temperate regions that experienced significant vegetation changes between 1870 and 1992, including both North America and west Eurasia (land areas within the dashed box in Fig. 2b). The monthly mean reconstructed albedo shows a seasonal cycle that follows fairly well the original MODIS albedo data. The reconstructed albedo however slightly overestimates the observed values during most part of year, with a mean bias of about 0.002 ($\sim$ 1 % of the observed mean albedo). This bias results from those regions showing systematically significant errors (Fig. 3), contributing to a mean absolute error (MAE) of around 5 % in all seasons (the MAE, indicated by shaded areas in Fig. 4, is calculated from the ensemble of grid-cells within the selected region).

3.2 Albedo changes between 1870 and 1992

As described in Sect. 2, seven pairs of MODIS-based albedo reconstructions were calculated for each of the seven LUCID LSM-specific present-day (1992) and preindustrial (1870) land-cover distributions. As with the simulated albedo, the MODIS-based estimated change in surface albedo was computed for each model as the difference between the present-day (PD) and preindustrial (PI) climatologies of the reconstructed dataset.

BGD
9, 12505–12542, 2012

The simulated and reconstructed mean LCC-induced albedo differences (PD minus PI) in January and July are displayed in Fig. 5. In both the simulated and reconstructed cases, the multi-model mean albedo change is displayed. Both the LUCID average modeled albedo and the reconstructed albedo maps show clear albedo increases over areas that have experienced the most intense deforestation between 1870 and 1992 (Fig. 2b). In January, the albedo increases between PI and PD reach more than 10 % (absolute) in some areas, around five times larger than those simulated in July. This difference results from the forest canopy snow-masking effect on albedo, which was larger in pre-industrial conditions when forests cover more area. The simulated mean albedo differences are very similar to the reconstructed one although slightly weaker in January and larger in July.

The consistency shown by the model-mean simulated and reconstructed albedo responses to LCC masks significant discrepancies when looking at each model individually. For each of the LUCID GCM/LSMs, Fig. 6 illustrates the simulated and reconstructed changes between PI and PD in seasonally varying albedo averaged over the region studied of maximum LCC (Fig. 2b). All models simulate a similar seasonal albedo change pattern characterized by marked maximum increases during the cold snowy season (black lines in Fig. 6). The amplitudes of the albedo anomalies between the winter and the summer are however quite at variance from one model to another. For example, CCAM/CABLE simulates null albedo changes between PI and PD in summer and near +2 % (absolute) in winter, while the ARPEGE/ISBA simulates albedo increases ranging from ∼ +1 % in summer to more than +5 % in winter. This is partly related to the different deforestation rates prescribed in each LUCID LSMs, as discussed in de Noblet-Ducoudré et al. (2012) and Boisier et al. (2012).

Besides the differences between the model's albedo responses to LCC, strong discrepancies exist between the simulated and reconstructed albedo anomalies (the latter are illustrated as dashed lines in Fig. 6). The reconstructed winter albedo changes between PI and PD overestimate those simulated for five GCM/LSMs (CCAM/CABLE, CCSM/CLM, ECHAM5/JSBACH, IPSL/ORCHIDEE

BGD
9, 12505–12542, 2012

and SPEEDY/LPJmL) and underestimate them for two models (ARPEGE/ISBA, ECEARTH/TESSEL). Four models also show marked discrepancies between the reconstructed and simulated summer (snow-free) albedo changes (ARPEGE/ISBA, CCAM/CABLE, ECEARTH/TESSEL and SPEEDY/LPJmL).

Table 3 summarizes the annual mean albedo changes averaged over the global ice-free lands (i.e. excluding Antarctica and Greenland). The simulated model-mean albedo increases by 0.51 % in response to increased (prescribed) crop and pasture areas between 1870 and 1992, globally. This simulated model-mean response to LCC includes all biogeophysical effects of LCC on climate. It hides quite different individual model responses ranging from 0.1 % (CCAM/CABLE) to 0.97 % (ECEARTH/TESSEL), i.e. an inter-model range (0.87 %) larger than the model-mean albedo response. The model-mean albedo change derived from the "data-driven" reconstructions is similar to the simulated change, but the associated inter-model range is more than halved (0.33 %). As the reconstructed values isolate the sole contribution of the different land-cover maps to the model dispersion, this result suggests that the role of the land surface parameterizations, the simulated background climate (e.g. the snow cover during PI and PD periods) and atmospheric feedbacks play on the resulting albedo responses to LCC is of critical importance in explaining the differences in simulated albedo change between PI and PD in the LUCID models.

Given that the land cover prescribed in each single GCM/LSM is the same as the one used for the corresponding albedo reconstruction, each model's albedo sensitivity to LCC can be quantified by the difference between each simulated and reconstructed LCC-induced changes. This difference is principally explained by two causes. First, the distinct snow-cover extension simulated by each model with respect to that uniformly prescribed in the reconstructions (NSIDC). A related factor that also contributes to the simulated albedo responses to LCC, which is not taken into account in the reconstructions, is the change in the snow cover and content between the two periods simulated. Such change, which could result from, e.g. a positive snow-albedo feedback, was however not identified as a significant driver of the winter albedo responses to LCC within

BGD
9, 12505–12542, 2012

the LUCID simulations (Boisier et al., 2012). The second main cause behind the differences between the simulated albedo changes and the reconstructed ones is the inherent albedo sensitivity to land cover perturbations for a given snow cover condition, which directly depends on the LSMs parameterizations and may differ from the one derived from MODIS data. Land surface albedo parameterizations are responsible for the summer (snow-free) albedo responses to LCC, and should partially contribute for the winter ones. The relative role of these inherent LSM parameterization-related albedo sensitivities vs. the snow coverage in the simulated winter albedo sensitivities are examined in the following section.

3.3 Evaluating LUCID model's snow cover and the albedo sensitivity to LCC

In order to evaluate the snow cover and snowpack simulated by the various GCM/LSMs, we compared their modeled snow extent and the snow water equivalent (SWE) values in the region studied (North America and Eurasia; dashed box in Fig. 2b). Figure 7a gives the simulated winter (DJF) area within this region covered by a snowpack with SWE equal or larger than the level indicated in x-axis. The snow coverage and content relation derived from the NSIDC data is also plotted as reference (dashed lines in Fig. 7a). In the models as well as in the NISDC dataset, most part of the region we are looking at (that totalizes nearly 25 million km^2) is covered with snow of at least 1 mm in DJF. The area decays asymptotically when increasing SWE and, e.g. no model shows an area larger than 7 million km^2 covered with a snowpack of 80 mm or deeper. More specifically, three GCM/LSMs, ECEARTH/TESSEL, ECHAM5/JSBACH and SPEEDY/LPJmL, clearly simulate too small snow extent at different given SWE levels with respect to what is diagnosed from the NISDC data, while ARPEGE/ISBA clearly overestimates it. CCAM/CABLE and CCSM/CLM simulate larger than observed snow covered areas with relatively high SWE values (SWE $>$ 50 mm) .

Comparing this analysis with what is depicted in Fig. 6, it is clear that discrepancies in snow cover simulated and that used as input to the reconstruction method are not the sole accountable for the differences between the simulated and reconstructed

BGD
9, 12505–12542, 2012

LCC-induced changes in albedo. For instance, IPSL/ORCHIDEE shows a quite good concordance in terms of snow content and extent with respect to reference dataset, buts its change in surface albedo between PI and PD nevertheless overestimate the reconstructed ones in winter.

To evaluate the albedo's sensitivity to LCC independently from the magnitude of the land-cover perturbation we use normalized anomalies. These are calculated as the net surface albedo change between 1870 and 1992 ($\Delta\alpha$) divided by the corresponding difference in the total fraction of herbaceous vegetation ΔF_{H} (i.e. $\Delta F_{\mathrm{CROPS}} + \Delta F_{\mathrm{GRASS}}$):

$$\Delta_{\mathrm{N}}\alpha = \frac{\Delta\alpha}{\Delta F_{\mathrm{H}}}. \quad (2)$$

This coefficient therefore represents the expected albedo change induced by total deforestation when both the barren soil fraction and snowpack are kept constant (few grid-cells within the LUCID models show significant changes (> 5 %) in bare soil fraction and are excluded in the analysis, as well as those pixels showing absolute SWE changes larger than 10 mm since pre-industrial times).

The $\Delta_{\mathrm{N}}\alpha$ simulated by each GCM/LSM are plotted as a function of SWE in Fig. 7b. The results are illustrated as moving averages over SWE windows of 15 mm, along with the range of one standard deviation calculated over the same SWE windows (shaded area in Fig. 7b). The reconstructed $\Delta_{\mathrm{N}}\alpha$ values are also plotted as a reference in Fig. 7b (dashed lines). This figure clearly shows how much the models differ in their albedo response per unit of area deforested, although the magnitude of $\Delta_{\mathrm{N}}\alpha$ increases with SWE in all of them. ARPEGE/ISBA and ECEARTH/TESSEL show the strongest albedo sensitivity to deforestation when compared to all other models and to the reconstructed values. This is consistent with their large winter albedo responses to LCC described in the previous section (Fig. 6). This holds in the case of ECEARTH/TESSEL despite the lower snow coverage simulated by this model in the selected region (Fig. 7a). The simulated $\Delta_{\mathrm{N}}\alpha$ in the other five models underestimate those reconstructed at different SWE levels. The weak albedo change simulated by CCAM/CABLE in winter (less than

BGD
9, 12505–12542, 2012

half of its associated reconstructed values) is consistent with the extremely low albedo sensitivity to LCC of this model.

The uneven winter albedo sensitivities to deforestation depicted in Fig. 7b reflect differences in land surface albedo parameterizations within the LUCID GCM/LSMs. As described above, these model sensitivities, independently from their simulated snow cover, are explaining an important fraction of the differences between the simulated and reconstructed winter LCC-induced albedo anomalies. To attribute these differences to either the albedo's sensitivity to deforestation or to the simulated snow cover/content, for each GCM/LSM we have plotted in Fig. 8a the relative error of the simulated winter (DJF) albedo response to LCC ($\Delta\alpha_{mod}$) with respect to that reconstructed ($\Delta\alpha_{rec}$) against the winter mean SWE. We use the relative error in $\Delta\alpha$ [defined by $(\Delta\alpha_{mod} - \Delta\alpha_{rec}) / \Delta\alpha_{mod}$] in order to avoid the differences between the models due to their specific LCC strength. As well as Fig. 8a and b illustrates the relative errors of $\Delta\alpha$ but plotted against the normalized albedo anomaly ($\Delta_N\alpha$; see Eq. 2) averaged at different SWE levels (i.e. this figure thus shows the "intrinsic" albedo sensitivity of each model independently from snow cover). No clear relationship was found in the first case (Fig. 8a), implying that the simulated snow does not dominate the relative $\Delta\alpha$ errors. In contrast, an approximately linear relationship appears in the second case (Fig. 8b).

The reconstructed mean $\Delta_N\alpha$ of near 0.3 (dashed line in Fig. 8b) is consistent with the mean snow-covered albedo difference between forest and herbaceous vegetation found in this study (Table 2) and similar to the strength of the snow-masking effect reported earlier (e.g. Bonan, 2008). The two models that overestimate this value (ARPEGE/ISBA and ECEARTH/TESSEL) simulate a higher albedo response to LCC than that reconstructed, while the others models underestimate it. Hence, the intrinsic LSM albedo's sensitivities to deforestation and, therefore, related to the land surface parameterizations, appear as the major factor explaining their differences in winter mean albedo responses to LCC.

The effect of snow content may be distinguished as a secondary component in Fig. 8b. Based on the linear fit between $\Delta_N\alpha$ and the departures of the winter mean

BGD
9, 12505–12542, 2012

albedo responses (dashed line), those models that simulate more (ARPEGE/ISBA) and less (ECEARTH/TESSEL, ECHAM5/JSBACH, SPEEDY/LPJmL) snow than the reference data (NSIDC) respectively overestimate and underestimate their expected albedo responses based on their mean $\Delta_N\alpha$.

Figure 8c illustrates the normalized 2-m temperature ($\Delta T_{2m} / \Delta F_H$) responses to LCC simulated in DJF as function of the mean $\Delta_N\alpha$. In this season and region (North America and Eurasia) all the models simulate cooling of amplitude roughly proportional to the increase in surface albedo and, then, proportional to the mean $\Delta_N\alpha$. Hence, those models showing weak albedo sensitivities to deforestation (e.g. CCAM/CABLE) simulate almost null temperatures responses, while e.g. ECEARTH/TESSEL, with a mean $\Delta_N\alpha$ of ~0.37, shows a cooling exceeding 3 K. The MODIS-based mean $\Delta_N\alpha$ of ~0.3 projected on the linear fit between the simulated $\Delta T_{2m} / \Delta H_H$ and the mean $\Delta_N\alpha$ values (dashed lines in Fig. 8c), brings an estimated temperature response to total deforestation of around −2.5 K.

3.4 Impacts on the surface shortwave radiation budget

The importance of large-scale surface albedo changes on climate resides on their resulting impacts on the surface radiation budget and, then, on the energy balance. The LCC-induced changes in surface net shortwave radiation (S_N) not only depend on the surface albedo changes ($\Delta\alpha$), but also on indirect impacts of LCC and atmospheric feedbacks that, by means of perturbations in e.g. convection and cloud cover, might induce changes in the incoming solar radiation (S_D). In order to isolate the albedo-driven (α-driven) component in the LCC-induced change in S_N (ΔS_N) from the preindustrial period S_N (PI) to present-day S_N (PD), we use the following decomposition:

$$\Delta S_N = S_N(\mathrm{PD}) - S_N(\mathrm{PI}) = -\Delta\alpha\, S_D(\mathrm{PI}) + [1 - \alpha(\mathrm{PI})]\, \Delta S_D - \Delta\alpha\, \Delta S_D. \quad (3)$$

The first term in the right-hand side of Eq. (3) represents the α-driven S_N change, while the second term is the "indirect" S_D-driven component briefly described above. The third term is an anomaly of second order (interactions between albedo and atmospheric

BGD
9, 12505–12542, 2012

feedback effects) that is negligible compared to the other terms when the perturbations are small compared to the net values (as in this case).

Figure 9 illustrates, for each of the LUCID models, the LCC-induced monthly S_N changes, averaged over the region studied in North America and Eurasia. The simulated S_N responses to LCC (indicated by solid lines in Fig. 9) are depicted along with the simulated (dotted lines) and reconstructed (dashed lines) α-driven ΔS_N. The latter are computed by evaluating the first term of Eq. (3) with the corresponding MODIS-based reconstructed $\Delta\alpha$ value, maintaining in each case the simulated S_D (PI).

Most models simulate decreases in S_N that exceed $5\,W\,m^{-2}$ in some cases (solid lines in Fig. 9). They also show very different seasonal patterns within their responses and, in most cases, quite different anomalies than those expected from the corresponding surface albedo changes (dotted lines). ARPEGE/ISBA is a clear exception regarding the latter. In this model, the simulated ΔS_N is led by the α-driven component, indicating comparatively weak changes in S_D. Differences between the net ΔS_N and the α-driven component are not systematic among the different models but some patterns prevail. During the winter (DJF), most models simulated similar or weaker net ΔS_N than those expected from $\Delta\alpha$ alone. The opposite pattern, i.e. larger decreases in S_N than those induced by $\Delta\alpha$, is seen in most models in JJA with the clear exception of SPEEDY/LPJmL. The latter shows particularly large increases in S_D leading to net increases in S_N in May–June between PI and PD. These results suggest that the indirect impacts of LCC by means of changes in the S_D play quite an important role in the simulated S_N changes in response to LCC changes between PI and PD. Within the various LUCID models, this effect differs in amplitude and, in some cases in sign, amplifying or dampening the direct (α-driven) S_N perturbations.

Except for ECHAM5/JSBACH all models show larger changes in α-driven S_D reduction during the winter and spring than in summer (dotted lines in Fig. 9), as we get in the reconstructions (dashed lines). The seasonal pattern of the simulated and reconstructed α-driven ΔS_D is however quite different for most models (except for IPSL/ORCHIDEE). For instance, in the case of ECEARTH/TESSEL, the

BGD
9, 12505–12542, 2012

difference between the simulated and reconstructed surface albedo change under snow-free conditions (Fig. 6) lead to a substantially overestimated α-driven decrease in S_N with respect to the MODIS-based reconstruction from May to October. A similar effect occurs with ARPEGE/ISBA and SPEEDY/LPJmL. In turn, the simulated α-driven S_N changes underestimate those reconstructed during most part of the year for CCSM/LSM, ECHAM5/JSBACH, IPSL/ORCHIDEE and CCAM/CABLE, in accordance to their differences between the reconstructed versus the simulated albedo changes (Fig. 6).

The global land annual mean LCC-induced changes in S_N are summarized in Table 4. As for the data shown in Fig. 9, the simulated net ΔS_N values and the α-driven components computed from both the simulated and the reconstructed $\Delta\alpha$, are indicated. The simulated model-mean ΔS_N between PI and PD is near $-0.9\,W\,m^{-2}$ with a large inter-model range of $1.21\,W\,m^{-2}$. The global land α-driven change in S_N is lower in amplitude than the total S_N changes when averaged across the models ($-0.75\,W\,m^{-2}$). The models differ between each other in their individual total S_N responses compared to their α-driven ΔS_N, and the inter-model range of this component of $1.44\,W\,m^{-2}$, i.e. twice as large as the its model-mean response. Consistent with what is obtained for the surface albedo (Table 3), the inter-model range of the MODIS-based reconstructed α-driven ΔS_N is strongly reduced from that simulated ($0.62\,W\,m^{-2}$), highlighting the major contribution of differences in land-surface parameterization in explaining the simulated albedo responses to LCC and the resulting spread between the models.

Averaged over the whole globe, the LUCID models show a annual mean S_N difference between PI and PD of $-0.16\,W\,m^{-2}$ (total simulated). Considering the α-driven component only, the model-mean S_N change is $-0.14\,W\,m^{-2}$ (simulated) and $-0.12\,W\,m^{-2}$ when using the reconstructed albedo change. These values are coherent with what Matthews et al. (2003) reported. They found a change in S_N larger in amplitude ($-0.15\,W\,m^{-2}$) using a crop albedo of 0.17 (i.e. higher, in average, than the crop albedo used in this study; Table 2) for a LCC from the pre-agricultural times

BGD
9, 12505–12542, 2012

(1700) to present-day (1992). Their simulated ΔS_N is almost twice when crop albedo is prescribed to 0.20, highlighting the large sensitivity of the radiative impact of LCC to land-surface parameterization.

The global mean ΔS_N found in this study are also within the typical radiative forcing (RF) of $-0.2 \pm 0.2\,W\,m^{-2}$ attributed to the past LCC due to surface albedo changes in previous modeling studies (Forster et al., 2007; Davin et al., 2007) and higher in amplitude than the RF of $-0.09\,W\,m^{-2}$ that was estimated by Myhre et al. (2005) from satellite observations. The change in S_N is however a quite rough estimation of the LCC-induced RF, which is usually computed at the top of the troposphere and, therefore, accounts for the net changes in shortwave radiation due to combined surface and cloud cover perturbations, in addition to changes in longwave radiation as indirectly perturbed by LCC via atmospheric feedbacks. The net impact of LCC in terms of RF could also be amplified by positive feedbacks due to changes in, e.g. the water vapor (Davin et al., 2007).

4 Discussion and conclusions

Results from the LUCID model intercomparison project have demonstrated that changes in surface albedo were one of the main drivers of the GCMs' responses to historical land-use induced land cover changes (LCC). This initiative has also showed that the simulated albedo change was quite different from one model to another. It then became important to evaluate the magnitude of this albedo response to historical LCC based on available observations.

In addition we have to recall that there is no current consensus on the intensity of past deforestation and, consequently, this aspect represents one of the main sources of uncertainty when comparing various studies addressing the impacts of LCC on climate (de Noblet-Ducoudré et al., 2012; Boisier et al., 2012).

We have used satellite-based surface albedo, land-cover and snow-cover data to derive snow-free and snow-covered monthly climatologies of albedo for five main land

BGD
9, 12505–12542, 2012

cover groups (LCGs). Those climatologies can be combined with any vegetation and snow cover distribution to reconstruct global albedo maps and then estimate LCC-induced albedo changes. We have used this methodology to assess changes in surface albedo since preindustrial times. Reconstructed albedos for both time periods used the land-cover maps provided by the seven GCM/LSMs that have been run in the context of the LUCID project. Preindustrial simulations and reconstructions only differ from present-day ones by the land-cover maps. The reconstructions were then compared to the albedo values simulated by each individual GCM/LSM to evaluate how realistic each model is with respect to the response of this specific variable to LCC.

It is important to note that the reconstructed preindustrial albedo maps use the present-day snow-cover data and LCG's monthly albedos. Thus, the resulting surface albedo change between 1992 and 1870 represents a first estimate of land-cover perturbation, i.e. prior to any climate feedback that could further modulate the albedo responses to LCC. However, our previous analyses of LUCID simulations show rather weak positive snow-albedo feedback (Boisier et al., 2012).

The LUCID models do not exhibit a systematic bias in their simulate albedo responses to LCC with respect to those reconstructed using the MODIS albedo and the NSIDC snow cover data. However, single model responses are significantly different from their respective reconstructions, notably when snow is present. We show that these differences reside principally on the land surface parameterizations of albedo which is summarized in the LSMs' albedo sensitivities to deforestation, while differences in snowpack simulated by the LUCID GCMs represent a secondary component of their winter albedo changes between pre-industrial and present. It should be noted that the winter temperature responses to LCC simulated by the LUCID models are mainly directed by surface albedo changes and, consequently, depend directly on the albedo sensitivity of LSMs (Fig. 8c).

The large dispersion in albedo responses to LCC shown by LUCID models echoes the reported uncertainty in the radiative forcing of past LCC (Forster et al., 2007). Our results show that the spread in the simulated albedo changes is in its major part

BGD
9, 12505–12542, 2012

associated to the LSMs' parameterizations, reinforcing previous conclusions from LUCID (Boisier et al., 2012). The remaining uncertainty is mainly related to the choice of land-cover maps. The indirect impacts of land-cover perturbations, inducing changes in the incoming solar radiation, are also quite model-dependent, adding additional uncertainty to the radiative effect of LCC.

Narrowing the large uncertainties in regional climate responses to LCC is a major challenge to move forward in the understanding of past climate trends and future projections, and will help other studies such as the climate change detection and attribution. Novel observation-based global products are a useful data source that could help to this purpose and notably be used as benchmark in climate modeling studies. Further, the methodology applied here may be used to estimated either past or future LCC-related changes in surface albedo, as well as in any other surface quantity that is available globally at relatively high resolution.

Acknowledgements. We thank the climate modeling groups participating in LUCID for providing model data and support. This research was partially funded by the Chilean National Commission for Scientific and Technological Research (CONICYT) and the EU-FP7 project AMAZALERT. The computing time was provided by the Commissariat à l'Energie Atomique (CEA), France. The MODIS MCD43C3 and MCD12C1 data were obtained through the online Data Pool at the NASA Land Processes Distributed Active Archive Center (LP DAAC), USGS/Earth Resources Observation and Science (EROS) Center, Sioux Falls, South Dakota (http://lpdaac.usgs.gov/get_data). The AVHRR/SMMR/SSM/I snow cover and snow water equivalent product (NSIDC-0271) were obtained from the National Snow and Ice Data Center (NISDC) Distributed Active Archive Center (DAAC).

The publication of this article is financed by CNRS-INSU.

BGD
9, 12505–12542, 2012

References

Abramowitz, G., Leuning, R., Clark, M., and Pitman, A.: Evaluating the performance of land surface models, J. Climate, 21, 5468–5481, 2008.

Armstrong, R. L., Brodzik, M. J., Knowles, K., and Savoie, M.: Global Monthly EASE-Grid Snow Water Equivalent Climatology, National Snow and Ice Data Center, Digital media, Boulder, Colorado, USA, 2007.

Betts, R. A.: Biogeophysical impacts of land use on present-day climate: near-surface temperature and radiative forcing, Atmos. Sci. Lett., 2, 39–51, doi:10.1006/asle.2001.0023, 2001.

Betts, R. A., Falloon, P. D., Klein Goldewijk, K., and Ramankutty, N.: Biogeophysical Effects of Land Use on Climate: Model Simulations of Radiative Forcing and Large-Scale Temperature Change, Agr. Forest Meteorol., 142, 216–233, 2007.

Boisier, J. P., de Noblet-Ducoudré, N., Pitman, A. J., Cruz, F. T., Delire, C., van den Hurk, B. J. J. M., van der Molen, M. K., Müller, C., and Voldoire, A.: Attributing the impacts of land-cover changes in temperate regions on surface temperature and heat fluxes to specific causes: Results from the first LUCID set of simulations, J. Geophys. Res., 117, D12116, doi:10.1029/2011JD017106, 2012.

Bonan, G. B.: Forests and climate change: Forcings, feedbacks, and the climate benefits of forests, Science, 320, 1444–1449, 2008.

Bondeau, A., Smith, P. C., Zaehle, S., Schaphoff, S., Lucht, W., Cramer, W., Gerten, D., Lotze-Campen, H., Müller, C., Reichstein, M., and Smith, B.: Modelling the role of agriculture for the 20th century global terrestrial carbon balance, Glob. Change Biol., 13, 679–706, 2007.

Bounoua, L., DeFries, R., Collatz, G. J., Sellers, P., and Khan, H.: Effects of land cover conversion on surface climate, Climatic Change, 52, 29–64, doi:10.1023/A:1013051420309, 2002.

Cescatti, A., Marcolla, B, Santhana Vannan, S. K., Yun Pan, J., Román, M. O., Yang, X., Ciais, P., Cook, R. B., Law, B. E., Matteucci, G., Migliavacca, M., Moors, E., Richardson, A. D., Seufert, G., and Schaaf, C. B.: Intercomparison of MODIS albedo retrievals and in situ measurements across the global FLUXNET network, Remote Sens. Environ., 121, 323–334, doi:10.1016/j.rse.2012.02.019, 2012.

Collins, W. D., Bitz, C. M. , Blackmon, M. L., Bonan, G. B., Bretherton, C. S., Carton, J. A., Chang, P., Doney, S. C., Hack, J. J., Henderson, T. B., Kiehl, J. T., Large, W. G., McKenna, D. S., Santer, B. D., and Smith, R. D.: The Community Climate System Model Version 3 (CCSM3), J. Climate, 19, 2122–2143. doi:10.1175/JCLI3761.1, 2006.

BGD
9, 12505–12542, 2012

Davin, E. L. and de Noblet-Ducoudré, N.: Climatic Impact of Global-Scale Deforestation: Radiative versus Nonradiative Processes, J. Climate, 23, 97–112, 2010.

Davin, E. L., de Noblet-Ducoudré, N., and Friedlingstein, P.: Impact of land cover change on surface climate: Relevance of the radiative forcing concept, Geophys. Res. Lett., 34, L13702, doi:10.1029/2007GL029678, 2007.

De Noblet-Ducoudré, N., Boisier, J. P., Pitman, A., Bonan, G., Brovkin, V., Cruz, F., Delire, C., Gayler, V., van den Hurk, B., Lawrence, P., van der Molen, M., Müller, C., Reick, C., Strengers, B., and Voldoire, A.: Determining robust impacts of land use induced land-cover changes on surface climate over North America and Eurasia; Results from the first set of LUCID experiments, J. Climate, 25, 3261–3281, doi:10.1175/JCLI-D-11-00338.1, 2012.

Feddema, J., Oleson, K., Bonan, G., Mearns, L., Washington, W., Meehl, G., and Nychka D.: A comparison of a GCM response to historical anthropogenic land cover change and model sensitivity to uncertainty in present-day land cover representations, Climate Dyn., 25, 581–609, 2005.

Forster, P., Ramaswamy, V., Artaxo, P., Berntsen, T., Betts, R., Fahey, D. W., Haywood, J., Lean, J., Lowe, D. C., Myhre, G., Nganga, J., Prinn, R., Raga, G., Schulz, M., and Van Dorland, R.: Changes in Atmospheric Constituents and in Radiative Forcing, in: Climate Change 2007: The Physical Science Basis. Contribution of Working Group I to the Fourth Assessment Report of the Intergovernmental Panel on Climate Change, edited by: Solomon, S., Qin, D., Manning, M., Chen, Z., Marquis, M., Averyt, K. B., Tignor, M., and Miller, H. L., Cambridge University Press, Cambridge, United Kingdom and New York, USA, 2007.

Gao, F., Schaaf, C. B., Strahler, A. H., Roesch, A., Lucht, W., and Dickinson, R.: MODIS bidirectional reflectance distribution function and albedo Climate Modeling Grid products and the variability of albedo for major global vegetation types, J. Geophys. Res., 110, D01104, doi:10.1029/2004JD005190, 2005.

Govindasamy, B., Duffy, P. B., and Caldeira, K.: Land use changes and Northern Hemisphere cooling, Geophys. Res. Lett., 28, 291–294, 2001.

Hansen, J. E., Sato, M., Lacis, A., Ruedy, R., Tegen, I., and Mathews, E.: Climate forcings in the Industrial era, PNAS, 95, 12753–12758, doi:10.1073/pnas.95.22.12753, 1998.

Jin, Y., Schaaf, C. B., Gao, F., Li, X., Strahler, A. H., Zeng, X., and Dickinson, R. E.: How does snow impact the albedo of vegetated land surfaces as analyzed with MODIS data?, Geophys. Res. Lett., 29, 1374, doi:10.1029/2001GL014132, 2002.

BGD
9, 12505–12542, 2012

Krinner, G., Viovy, N., de Noblet-Ducoudré, N., Ogée, J., Polcher, J., Friedlingstein, P., Ciais, P., Sitch, S., and Prentice, I. C.: A dynamic global vegetation model for studies of the coupled atmosphere-biosphere system, Global Biogeochem. Cy., 19, GB1015, doi:10.1029/2003GB002199, 2005.

Kvalevåg, M. M., Myhre, G., Bonan, G., and Levis, S.: Anthropogenic land cover changes in a GCM with surface albedo changes based on MODIS data, Int. J. Climatol., 30, 2105–2117, doi:10.1002/joc.2012, 2010.

Marti, O., Braconnot, P., Dufresne, J.-L., Bellier, J., Benshila, R., Bony, S., Brockmann, P., Cadule, P., Caubel, A., Codron, F., de Noblet, N., Denvil, S., Fairhead, L., Fichefet, T., Foujols, M.-A., Friedlingstein, P., Goosse, H., Grandpeix, J.-Y., Guilyardi, E., Hourdin, F., Krinner, G., Lévy, C., Madec, G., Mignot, J., Musat, I., Swingedouw, D., and Talandier, C.: Key features of the IPSL ocean atmosphere model and its sensitivity to atmospheric resolution, Clim. Dyn., 34, 1–26, doi:10.1007/s00382-009-0640-6, 2010.

Matthews, H. D., Weaver, A. J., Eby, M., and Meissner, K. J.: Radiative forcing of climate by historical land cover change, Geophys. Res. Lett., 30, 1055, doi:10.1029/2002GL016098, 2003.

McGregor, J. L. and Dix, M. R.: An updated description of the Conformal-Cubic Atmospheric Model, in: High Resolution Simulation of the Atmosphere and Ocean, edited by: Hamilton, K. and Ohfuchi, W., 51–76, Springer, New York, 2008.

Myhre, G. and Myhre, A.: Uncertainties in radiative forcing due to surface albedo changes caused by land-use changes, J. Climate, 16, 1511–1524, doi10.1175/1520–0442, 2003.

Myhre, G., Kvalevåg, M. M., and Schaaf, C. B.: Radiative forcing due to anthropogenic vegetation change based on MODIS surface albedo data, Geophys. Res. Lett., 32, L21410, doi:10.1029/2005GL024004, 2005.

Oleson, K. W., Niu, G.-Y., Yang, Z.-L., Lawrence, D. M., Thornton, P. E., Lawrence, P. J., Stöckli, R., Dickinson, R. E., Bonan, G. B., Levis, S., Dai, A., and Qian, T.: Improvements to the Community Land Model and their impact on the hydrological cycle, J. Geophys. Res., 113, G01021, doi:10.1029/2007JG000563, 2008.

Pitman, A. J., de Noblet-Ducoudré, N., Cruz, F. T., Davin, E. L., Bonan, G. B., Brovkin, V., Claussen, M., Delire, C., Ganzeveld, L., Gayler, V., van den Hurk, B. J. J. M., Lawrence, P. J., van der Molen, M. K., Müller, C., Reick, C. H., Seneviratne, S. I., Strengers, B. J., and Voldoire, A.: Uncertainties in climate responses to past land cover change:

BGD
9, 12505–12542, 2012

First results from the LUCID intercomparison study, Geophys. Res. Lett., 36, L14814, doi:10.1029/2009GL039076, 2009.
Raddatz, T., Reick, C. H., Knorr, W., Kattge, J., Roeckner, E., Schnur, R., Schnitzler, K. G., Wetzel, P., and Jungclaus, J.: Will the tropical land biosphere dominate the climate-carbon cycle feedback during the twenty-first century?, Clim. Dyn., 29, 565–574, 2007.
Roeckner, E., Brokopf, R., Esch, M., Giorgetta, M., Hagemann, S., Kornblueh, L., Manzini, E., Schlese, U., and Schulzweida, U.: Sensitivity of simulated climate to horizontal and vertical resolution in the ECHAM5 atmosphere model, J. Climate, 19, 3771–3791, 2006.
Salas-Mélia, D., Chauvin, F., Déqué, M., Douville, H., Guérémy, J. F., Marquet, P., Planton, S., Royer, J. F., and Tyteca, S.: Description and validation of the CNRM-CM3 global coupled climate model, Note 103, Centre du Groupe de Météorologiques de Grande Echelle et Clim., Toulouse, France, available at: http://www.cnrm.meteo.fr/scenario2004/paper_cm3.pdf, 30 September 2005.
Schaaf, C. B., Gao, G., Strahler, A. H., Lucht, W., Li, X., Tsang, T., Strugnell, N. C., Zhang, X., Jin, Y., Muller, J. P., Lewis, P., Barnsely, M. J., Hobson, P., Disney, M., Roberts, G., Dunderdale, M., Doll, C., D'Entremont, R. P., Hu, B., Liang, S., Privette, J., and Roy, D. P.: First operational BRDF, albedo nadir reflectance products from MODIS, Remote Sens. Environ., 83, 135–148, 2002.
Strengers, B. J., Muller, C., Schaeffer, M., Haarsma, R. J., Severijns, C., Gerten, D., Schaphoff, S., van den Houdt, R., and Oostenrijk, R.: Assessing 20th century climate-vegetation feedbacks of land-use change and natural vegetation dynamics in a fully coupled vegetation-climate model, Int. J. Climatol., 30, 2055–2065, doi:10.1002/joc.2132, 2010.
van den Hurk, B. J. J. M., Viterbo, P., Beljaars, A. C. M., and Betts, A. K.: Offline validation of the ERA40 surface scheme, Tech. Memo., Eur. Cent. for Med.-Range Weather Forecasts, Reading, UK, 295, 43 pp., 2000.
Voldoire, A.: Quantifying the impact of future land-use changes against increases in GHG concentrations, Geophys. Res. Lett., 33, L04701, doi:10.1029/2005GL024354, 2006.

BGD
9, 12505–12542, 2012

Table 1. Dataset summary.

Sources	Variables[a]	Period
MODIS (LP DAAC)	α, SC, LC	2000–2011
AVHRR/ SMMR/ SSM/I (NSIDC)	SC, SWE	1979–2006
LUCID simulations (7 GCM/LSMs[b])	α, LC, SC, SWE, S_N, S_D, T_{2m}	30-yr runs (5 ensemble members) with prescribed SST/SIC from 1970 to 1999. LC: 1870 (PI) and 1992 (PD)

[a]Surface albedo (α), snow cover fraction (SC), land cover (LC), snow water equivalent (SWE), net (S_N) and downward (S_D) shortwave radiation at the surface and 2-m temperature (T_{2m}).

[b]GCM/LSMs: ARPEGE/ISBA (Salas-Mlia et al., 2005; Voldoire et al., 2006), CCAM/CABLE (McGregor and Dix, 2008; Abramowitz et al., 2008), CCSM/CLM (Collins et al., 2006; Oleson et al., 2008), ECEARTH/TESSEL (van den Hurk et al., 2000), ECHAM5/JSBACH (Roeckner et al., 2006; Raddatz et al., 2007), IPSL/ORCHIDEE (Marti et al., 2010; Krinner et al., 2005) and SPEEDY/LPJmL (Strengers et al., 2010; Bondeau et al., 2007).

BGD
9, 12505–12542, 2012

Table 2. MODIS seasonal mean shortwave broadband (0.3–5 µm) directional hemispherical reflectance (black-sky albedo) in the northern temperate regions (30–60° N) for the five land cover groups used in this study.[a]

Land cover group	DJF (SC)	DJF (SF)	JJA (SF)
Crops	0.59 ± 0.07	0.15 ± 0.03	0.15 ± 0.02
Grasses	0.61 ± 0.07	0.19 ± 0.03	0.16 ± 0.02
Evergreen trees	0.22 ± 0.05	0.10 ± 0.02	0.09 ± 0.01
Deciduous trees	0.29 ± 0.04	0.12 ± 0.02	0.12 ± 0.02
Bare soil	0.59 ± 0.08	0.26 ± 0.07	0.26 ± 0.07

[a]The mean ±1 standard deviation are indicated for snow-covered (SC) and snow-free (SF) surface albedo values of the ensemble of grid cells (at 0.05 degree resolution) with dominant land cover (areal fraction > 95 %) within the 30–60° N latitude band.

BGD
9, 12505–12542, 2012

Table 3. Global land (ice-free) annual mean LCC-induced change in surface albedo (×100).

	models							
	ARP.	CCA.	CCS.	ECE.	ECH.	IPS.	SPE.	mean (range)
Simulated	0.64	0.10	0.22	0.97	0.28	0.49	0.85	0.51 (0.87)
Reconstructed	0.48	0.55	0.30	0.63	0.36	0.63	0.55	0.50 (0.33)

BGD
9, 12505–12542, 2012

Table 4. Global land (ice-free) annual mean LCC-induced changes in surface net shortwave radiation ($W\,m^{-2}$).

	models							
	ARP.	CCA.	CCS.	ECE.	ECH.	IPS.	SPE.	mean (range)
Simulated	−0.68	−1.53	−0.32	−1.10	−0.35	−0.52	−1.03	−0.89 (1.21)
α−driven (sim.)	−0.81	−0.04	−0.29	−1.41	−0.42	−0.79	−1.47	−0.75 (1.44)
α−driven (rec.)	−0.53	−0.53	−0.40	−0.80	−0.44	−1.01	−0.72	−0.63 (0.62)

BGD
9, 12505–12542, 2012

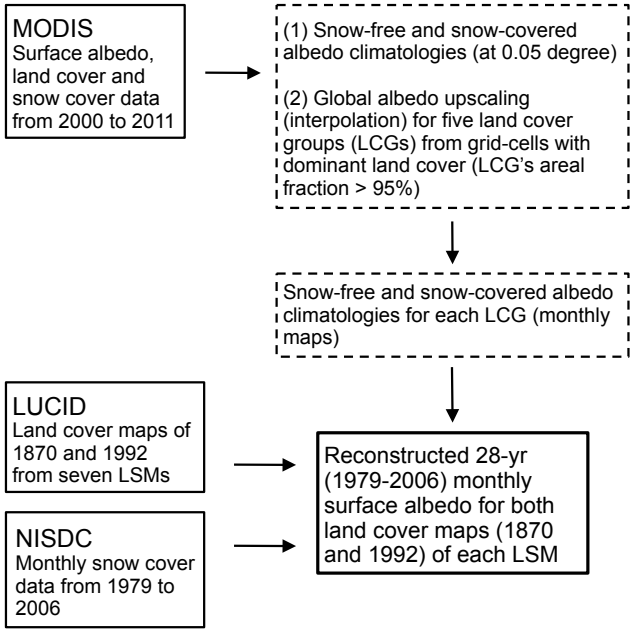

Fig. 1. Flowchart of the methodology used to compute surface albedo climatologies for land cover maps of 1870 and 1992 based on satellite data.

BGD
9, 12505–12542, 2012

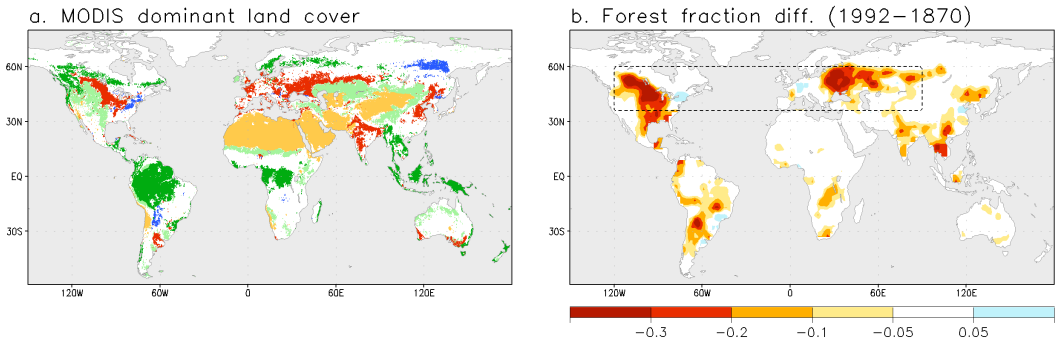

Fig. 2. (a) Grid-cells in a MODIS-based vegetation map (at 0.05-degree latitude-longitude) showing a dominant land cover (fraction of 95 % or larger) within the land cover groups used in this study: crops (red), grasses (lighter green), evergreen trees (darker green), deciduous trees (blue) and bare soil (orange). **(b)** Difference between the forest fraction of 1992 and 1870 prescribed in the LUCID LSMs' land cover maps (model mean). Box indicates the land areas of large deforestation in the northern extratropics further used for specific analyses.

BGD
9, 12505–12542, 2012

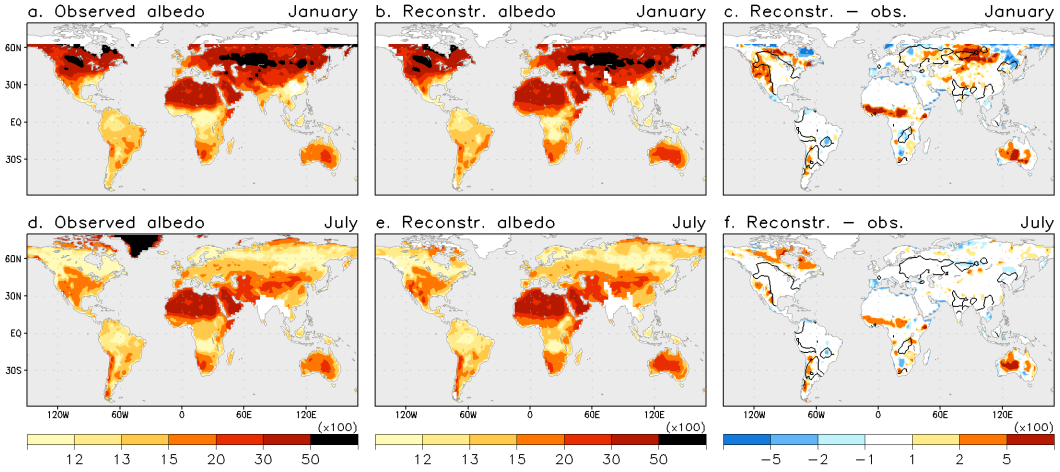

Fig. 3. Mean surface albedo in January (top) and July (bottom) based on MODIS (2000–2011) observations **(a, d)** and reconstructions **(b, e)**. Note the non-linear scale. Difference between the reconstructed and the observed albedo **(c, f)**. Solid contours encompass regions with areal fraction deforested larger than 10 % between 1870 and 1992.

BGD
9, 12505–12542, 2012

Inferring past land-use induced changes in surface albedo

J. P. Boisier et al.

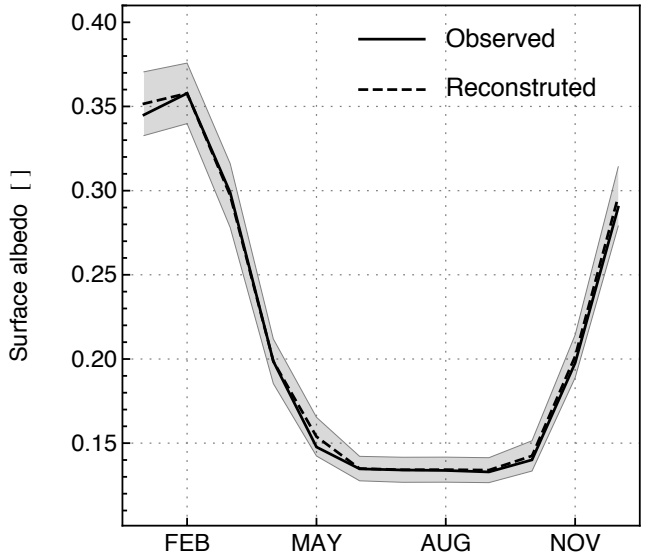

Fig. 4. Monthly mean albedo for North America and Eurasia (land areas within the dashed box indicated Fig. 2b). Solid and dashed lines indicate the observed and the reconstructed values, respectively. Shading indicates the reconstruction ± mean absolute error (MAE) between the reconstruction and the observation, calculated from the ensemble of grid-cells within the region studied.

BGD
9, 12505–12542, 2012

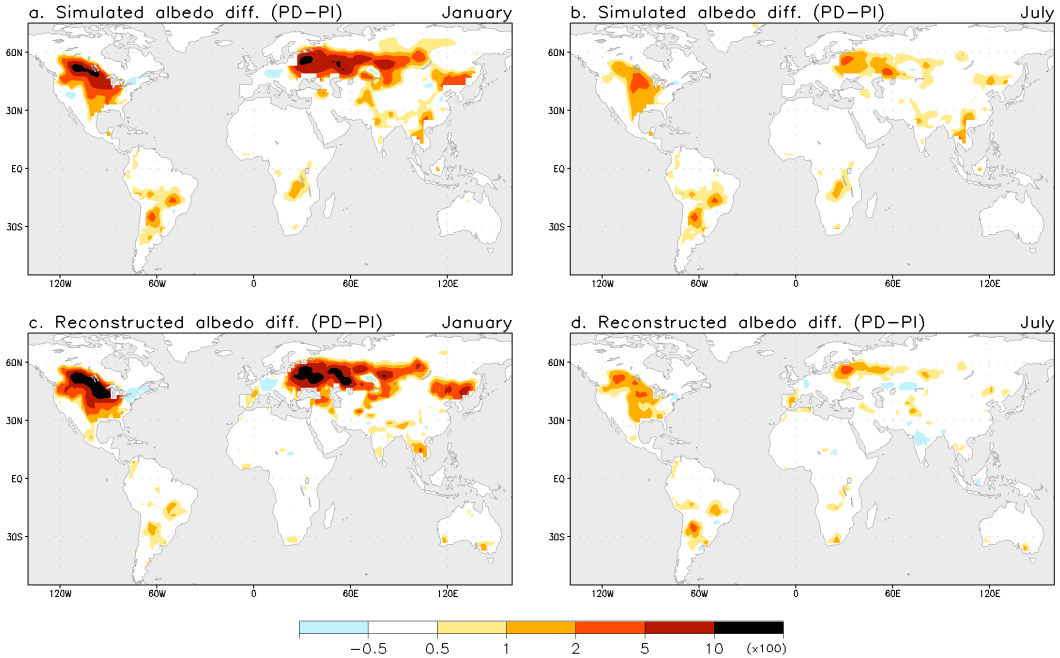

Fig. 5. LCC-induced surface albedo change in January **(a, c)** and July **(b, d)**. Model-mean change from LUCID simulations **(a, b)** and from reconstructions **(c, d)**. Note the non-linear scale.

BGD
9, 12505–12542, 2012

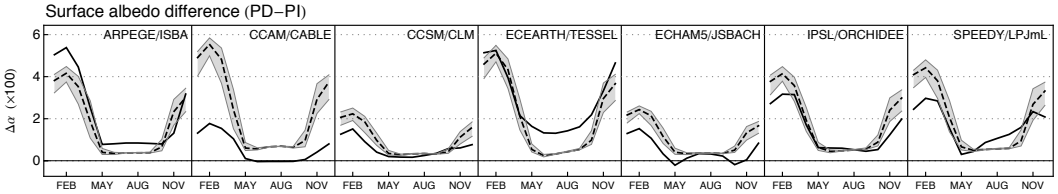

Fig. 6. Monthly mean surface albedo change for each LUCID model in the region studied (North America and Eurasia). Solid and dashed lines illustrate the simulated and the reconstructed albedo changes, respectively. Shaded area indicates the range between the minimum and maximum anomalies within the reconstructed single years (i.e. with minimum and maximum snow cover).

BGD
9, 12505–12542, 2012

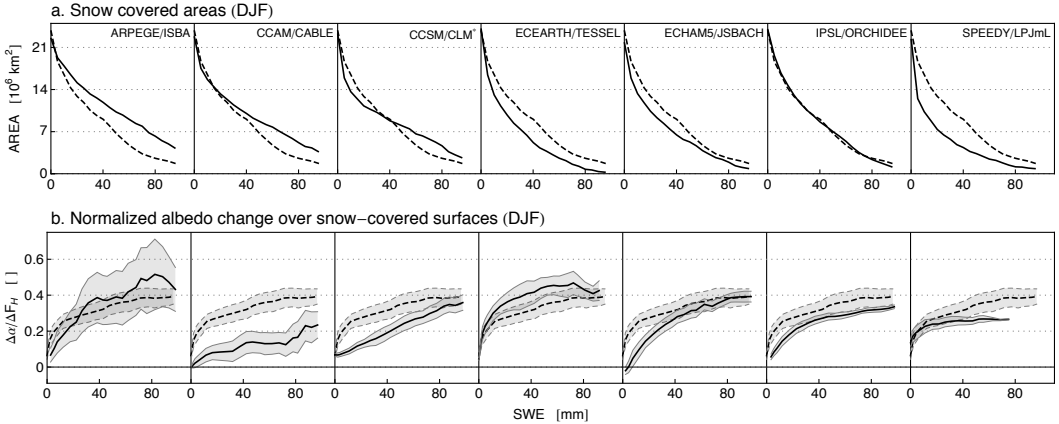

Fig. 7. (a) Snow covered area within the region studied (North America and Eurasia) in winter (DJF) with snow water equivalent (SWE) levels higher than the value indicated in the x-axis. Solid and dashed lines illustrate the results from LUCID models and from the NISDC data, respectively. **(b)** Normalized surface albedo changes ($\Delta\alpha / \Delta F_H$) averaged over SWE windows of 10 mm centered on the indicated values (see text). Simulated and reconstructed anomalies as solid and dashed lines, respectively. Shaded areas indicate the corresponding ±1 standard deviation at each SWE level.

BGD
9, 12505–12542, 2012

Inferring past land-use induced changes in surface albedo

J. P. Boisier et al.

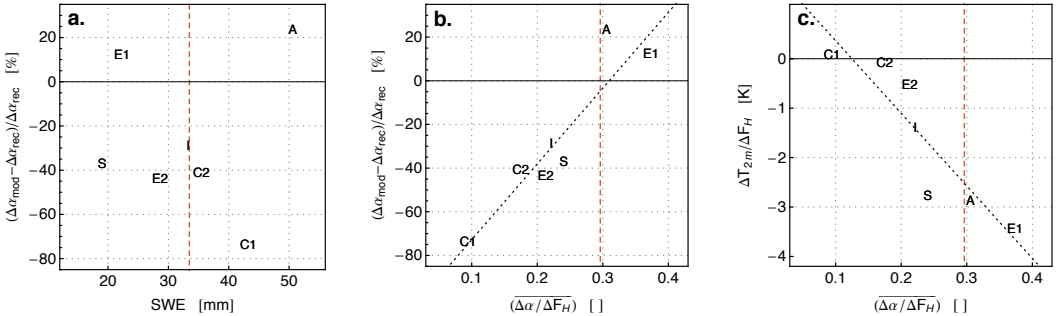

Fig. 8. Differences (relative, %) between the winter mean (DJF) reconstructed and simulated albedo responses to LCC in North America and Eurasia, plotted against the simulated mean SWE **(a)**, and plotted against the normalized albedo changes ($\Delta\alpha / \Delta F_H$) averaged at different snow cover contents **(b)**. Winter mean normalized 2-m temperature changes ($\Delta T_{2m} / \Delta F_H$) versus the mean $\Delta\alpha / \Delta F_H$ **(c)**. Dashed lines indicate the corresponding values obtained from the reference SWE dataset (NISDC) and the albedo reconstructions. Labels A, C1, C2, E1, E2, I and S indicate respectively ARPEGE, CCAM, CCSM, ECEARTH, ECHAM5, IPSL and SPEEDY.

BGD
9, 12505–12542, 2012

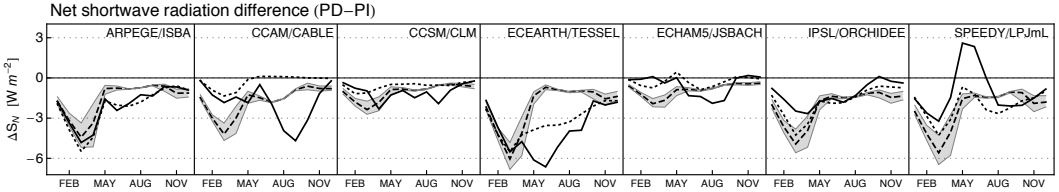

Fig. 9. As in Fig. 6 but for net shortwave radiation (S_N). Simulated total and albedo-driven (see text) changes in S_N as solid and dotted lines, respectively. Dashed lines indicate the albedo-driven S_N changes evaluated with the reconstructed (MODIS-based) changes in surface albedo.

BGD
9, 12505–12542, 2012